Available online at www.CivileJournal.org

Civil Engineering Journal

(E-ISSN: 2476-3055; ISSN: 2676-6957)

Vol. 9, No. 11, November, 2023

The Effect of Shear Stress on Armor Layer Thickness Under Steady Uniform Flow

Cahyono Ikhsan [1*]

[1] *Department of Civil Engineering, Faculty of Engineering, Universitas Sebelas Maret Surakarta, Indonesia.*

Received 06 July 2023; Revised 11 October 2023; Accepted 23 October 2023; Published 01 November 2023

Abstract

The armor layer is essential for maintaining stability on riverbed surfaces. This layer forms when bedload sediment moves until the bed's surface erodes, resulting in a stable layer that reaches an equilibrium state where no further sediment transport occurs. Therefore, the objective of this study is to investigate the effect of grain size and shear stress on armor layer thickness using evenly mixed sand and gravel with five different grain size variations. The research methodology consists of laboratory experiments and optimization analysis. The main instrument used is a sediment-recirculating flume constructed from plexiglass, measuring 10, 0.60, and 0.45 m in length, width, and height, respectively. Bed slope varies across gradients of 1%, 1.4%, 1.8%, 2.2%, and 2.6%. The constant flow rate is set at capacities of 25 l/s, 30 l/s, 40 l/s, and 45 l/s. The results show the consistent behavior of the channel bed surface under different flow rate variations. Meanwhile, the variables affecting armor layer thickness are the uniformity coefficient (C_u), the difference in shear stress on the bed surface ($\frac{\tau_o-\tau_c}{\tau_c}$), beds shear stress, and the critical shear stress of the sediment grain. The primary novelty of this research is a formula to determine armor layer thickness. It showed that both shear stress and the proportion of sand-to-gravel materials play significant roles in the armoring process and subsequent changes in the riverbed.

Keywords: Armor Layer Thickness; Bed Materials Grain Size; Flow Shear Stress; Flume.

1. Introduction

Natural changes in the riverbed are capable of significantly affecting the environment and structures within the river. These are caused by erosion and sedimentation processes, leading to either degradation or aggradation of the riverbed [1, 2]. The alterations in riverbed elevation are influenced by flow velocity and the transport of sediments, known as bedload [3, 4]. In principle, sediment transport is determined by various factors, including channel width, roughness, grain size, flow rate, shear stress on the channel bed, and stream power function [5–7]. The accurate measurement and estimation of bedload transport in the field are challenging due to the heterogeneous nature of materials and flow, limited information about initial and boundary conditions of sediment transport, spatial and temporal variations depending on flow conditions, nonlinearity, difficulties in obtaining suitable sediment measurement equipment, bedload hysteresis, and human activities. As a result, commonly used formulas for estimating sediment transport are derived from river samples and laboratory experiments [4, 7, 8]. Field observations show that individual unsteady flow events or flood hydrographs can greatly alter the morphology of the riverbed. Besides, a definitive formula to determine the extent of such changes has not yet been found. Changes in the riverbed texture occur rapidly due to variations in shear stress and the availability of sediment materials [9]. An investigation into how the armor layer formed was conducted by evaluating the channel bed change. To compare the two transport functions of MPM and WC, the MPM model provides larger

* Corresponding author: cahyonoikhsan@staff.uns.ac.id

http://dx.doi.org/10.28991/CEJ-2023-09-11-012

shear stresses than those of the WC model, particularly for deposition conditions. The WC model shows larger erosion on the bed change than the MPM model. After simulation, the median grain size provides a stable condition for all sampling materials and locations. It shows evidence that the active layer, which represents the mobile armor layer, has similar grain-size material along the channel [10].

Larger grain sizes typically characterize the riverbed layer compared to the underlying ones. The process of forming a rougher surface layer to protect the riverbed is called armoring [2, 11]. Furthermore, armoring significantly impacts channel hydraulics, sediment transport availability, habitat conditions for aquatic species, river geomorphology, turbulence, and riverbed degradation [12–14]. Its effect is particularly pronounced during floods with long-duration recession hydrographs, in contrast to flash floods [2]. Riverbed armor is categorized into two main types, namely static and mobile [13, 15, 16].

Static armor refers to a protective layer on the riverbed or channel when finer grain is selectively passed due to limited sediment supply from upstream [11, 17]. It can also occur when flow conditions result in insufficient shear stress to move the larger armor grain but can still transport smaller sizes [18]. This condition is commonly observed downstream of lakes or dams. Preliminary studies have reported several influencing factors, including grain size, flow depth and rate, sand content, and shear stress [19–21]. According to Ikhsan, an armor layer is formed when the finer sediments have been transported extensively, leaving behind relatively uniform coarser grain materials [22]. Its thickness is typically presented in non-dimensional terms.

Mobile armor is a protective layer that develops when the mobility difference between large and small grains decreases, resulting in greater exposure of larger grains to flow [23]. The concepts of both Static and Mobile Armor are shown in Figure 1. Prior studies on mobile armor reported that its structure is relatively unaffected by sediment transport rates, except under low transport conditions [19, 24]. The sediment composition on the channel bed highly influences the formation of the mobile armor layer and the resulting geometry. Additionally, variations in the initial surface shape greatly affect the response to its geometry. Wilcock & DeTemple [12] stated that the mobile armor layer formed during low flow tends to be persistent even during high flow. Understanding the protective layer that remains during low flow can simplify predictions related to sediment transport, hydraulic roughness, and habitat disturbance during flood events.

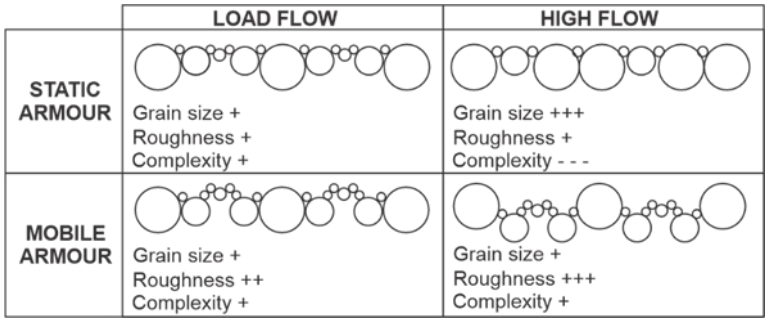

Figure 1. Concept of Static and Mobile Armor [19]

1.1. Armoring

Armoring can be defined as the process of forming an armor layer to protect a riverbed or channel from erosion. It begins with the breakage of the existing static armor, which exposes the underlying sand materials. As a result, the structure undergoes changes that close the gaps, forming a new one called mobile armor. Marion et al. [25] reported that two groups of grain scales are associated with this process. Slow formation conditions led to the creation of a stable bed that acts as static armor, while the reverse situation, caused by strong flow, contributed to the formation of mobile armor. It is worth noting that the grains in the mobile armor layer are smaller compared to those in the static armor layer [19]. The formation of clusters of gravel layers is crucial for protecting the riverbed [6]. During prolonged periods of low water flow (recession hydrographs), there is a higher likelihood of significant armor layer formation than sudden flash floods [2]. The armoring process in the channel bed is divided into two techniques, namely surface roughening and cluster formation. Shear stress encountered during the cluster formation process is higher than in the surface roughening technique [14].

Wang et al. [26] concluded that the formation degree of the channel bed structure influences the formation and reconstruction of the static armor layer. After the static armor layer has been developed, the surface layer forms a structure with different levels of particle aggregation and improves the stability of the layer. The level of influence of the bed structure on the stability of the channel bed can be obtained by eliminating two factors that affect the stability of the river bed, so-called the bed structure and the roughness of the channel bed. The median particle size ratio between the surface layer and the subsurface layer D_{50}/D_{50t} (armor ratio) is a value indicating the influence of the bed structure. In this study, dimensionless incipient shear stress is presented which is defined as the shear stress value at which the grain begins to move. These two parameters can be used as an estimation model to calculate the size distribution of static armor layers after riverbed protection reconstruction has taken place.

Marion & Fraccarollo [15] stated that the formation of the mobile armor layer and the channel bed geometry is significantly affected by the composition of sediment materials on the channel bed. Additionally, variations in the initial surface shape greatly affected the response to its geometry. They conducted laboratory flume experiments using bimodal and trimodal mixed sediments. The experiments revealed that the response to the channel bed geometry differed depending on the sediment mixture used. When bimodal sediments were employed, the formation of antidunes was observed, while trimodal materials resulted in changes in the mobility of coarse sand and middle materials. Elgueta-Astaburuaga & Hassan [16] stated the significance of the channel bed surface condition and sediment availability in controlling its transport conditions. It was further reported that channel bed degradation and aggradation cycles usually occur due to sediment supply from upstream, sediment discharge rate, topography, and channel bed composition. Significant changes in sediment supply typically drive large-scale cycles of degradation and aggradation. In contrast, the reverse phenomenon is more localized, influenced by changes within the channel bed.

Bedload transport refers to the movement of sediment where solid grain slide, roll, and hop close to the channel bed ($0 < z < z_{sb}$), as shown in Figure 2. When calculating bedload sediment transport, it is crucial to exercise caution due to the strong dependence of the equations on specific parameters. Therefore, it is important to carefully choose and apply the appropriate equations to ensure accuracy and reliability in estimating bedload sediment transport.

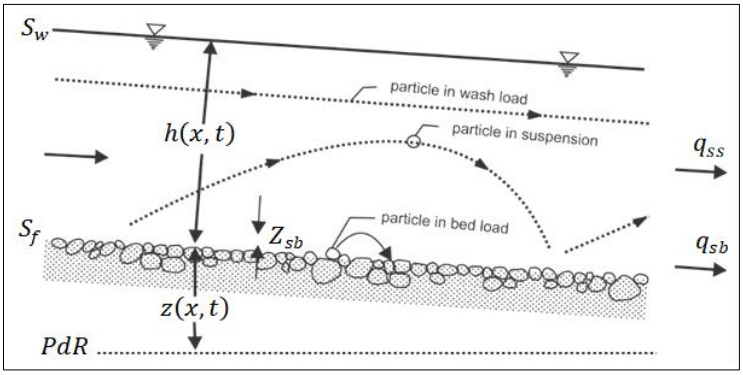

Figure 2. Scheme of Bedload Sediment Transport [27]

1.2. Layer of Armor

Several studies involving investigations in both laboratory and field settings have been conducted to explore the armor layer. In the field, a natural channel bed was often observed during the recession phase once water levels declined. The natural flow dynamics in rivers induce spatial variations in shear stress, consequently leading to corresponding spatial variations in grain size on both the surface and subsurface levels [28]. These findings emphasize the influence of flow variations on the distribution of grain size within natural river systems.

The empirical formula Raudkivi (1990) developed to predict the stability of the armor layer is stated in Equation 1.

$$\tau_{*cr} = \frac{\left(u_{*acr}\right)^2}{\left(s_s - 1\right) g\, d_{50_{a,max}}} \qquad (1)$$

$$d_{50_{a,max}} \leq 0.55\, d_{100}$$

where $d_{50_{a,max}}$ is median grain diameter of armor layer, and τ_{*cr} is non-dimensional critical shear stress ≈ 0.05.

A fraction of the largest grain primarily controls the formation of an armor layer in a channel, typically D_{90} or larger, present in the granulometric curve. It should be noted that assuming grain sizes are uniformly distributed, the armor layer would not develop [27]. In the equation, shear stress is only affected by the fraction of the median grain size (d_{50}), while the minimum size of specific grains that contribute to the armor layer remains uncertain. Furthermore, the effect of channel slope was accounted for in the armor formation process.

Chin et al. [11] conducted laboratory experiments to investigate the formation of armor layers using non-uniform sediments. A unique method that involved an adjustable sediment bed layer, enabling constant shear stress and uniform flow conditions throughout the experiments, was introduced. It was revealed that non-uniform sediments formed a stable armor layer within a specific shear stress range. Interestingly, the experiments also determined that the non-dimensional critical shear stress depended on the ratio of the maximum and median grain size of the sediments. The critical armor layer occurs at the lower boundary of the non-uniform sediment grain, while uniform sediments are not involved in its formation.

Wilcock et al. [29] stated that the sand content significantly influences the transport rates of course or gravel grain and the overall movement of sediments. In sediment mixtures consisting of sand and gravel, an increase in sand content

within the range of 15 to 27% triggers the transport rate of coarse grain. While variations in sand content affect the surface grain size, laboratory experiments have demonstrated minimal or slight impact on the surface roughening process corresponding to changes in flow magnitude and sediment transport rate. To quantify the total sediment transport rate in such mixtures, a non-dimensional parameter based on the median grain size (D_{50}), similar to Shields number (τ^*), can be used in Equation 2 as an indicator of grain motion initiation.

$$\tau^* = \frac{\tau}{(s-1)\rho g D_{50}} \quad (2)$$

Wilcock & DeTemple [12] conducted laboratory experiments using a surface-based transport model to investigate the behavior of armor layers formed during low-flow conditions in rivers. It was observed that the armor layer remained intact even during high-flow or flood conditions. This finding has significant implications as it simplifies sediment transport and hydraulic roughness estimation on the riverbed surface. Understanding that the armor layer persists during high-flow events makes it easier to predict and analyze sediment transport processes in rivers.

Extensive study has been conducted to examine the formation and disruption of the armor layer, composed of coarse gravel, on beds of the Ebro River during flood periods. The findings indicated that the magnitude of the flood event controls the degree of armoring occurring on the riverbed [30]. Further investigation revealed that floods can disrupt the armor layer, resulting in varying sediment patterns on the bed. This disruption occurs due to the powerful flushing flow during subsequent flood events. This highlights the importance of balanced sediment transport and supply along the river, particularly downstream of dams.

Viparelli et al. [31] developed a model to investigate the effect of flood flow and gravel addition on the fine sediment fraction in the uppermost layer of the river substrate. The study focused on the Trinity River in California and involved observing significant changes in its morphology. Furthermore, a one-dimensional numerical model called the Spawning Gravel Refresher was used to estimate and design the impacts of gravel augmentation on the riverbed. This approach facilitated simulations and assessments to understand better how adding additional gravel influenced the overall morphology of the river.

Curran & Waters [21] conducted laboratory experiments to investigate the surface structure of static armor layers formed under different flow rates and sand content conditions. It was reported that as the static armor layer develops, the complexity of the bed surface decreases. Notably, when the bed's surface layer contains more sand, the armor layer experiences significant adjustments. The composition of the sediment mixture and flow rate were identified as crucial factors influencing its characteristics. Importantly, the experimental data demonstrated that while the sediment mixture had a primary influence, flow rate acted as a secondary variable affecting the sand content during the formation process of the armor layer.

Spiller et al. [20] stated that several key factors influence the increase in dynamic lift on the static armor layer at the flow bed. Firstly, a decrease in the initial flow depth (initial) contributed to the increase in dynamic lift. Additionally, an increase in the lift value (ramping rate) represented as Δd/tR, and a decrease in the lift duration (ΔtR) were observed to have a positive effect on dynamic lift. An increase in flow discharge (ΔQ) at a constant ramping rate also increased dynamic lift. In laboratory experiments, it was demonstrated that an increase in channel bed porosity mitigated dynamic lift, thereby reducing its magnitude.

Powell et al. [24] conducted a study using a sediment-recirculating flume to investigate the structure of the mobile armor layer. It was reported that, overall, the structure of the armor layer is not significantly affected by the transport rate, except for lesser ones characterized by a non-dimensional shear stress magnitude of 0.03 When the grain scale ranges from 1 mm to 45 mm, with a median grain size (Ds50) between 9 mm and 17 mm, an increase in surface roughness, and a simplified complexity was observed. On the other hand, at a larger grain scale ranging from 100 mm to 200 mm, the study revealed additional surface layers at higher and lower elevations. These findings highlight the varying influences of grain size on the surface structure of the mobile armor layer.

Bertin et al. [32] conducted experiments in the flume to create a stable armor layer and examine the relationship between its properties and formative parameters. It was supported by extensive data from previous studies. The findings revealed that the topography or structure of the armor layer is highly responsive to changes in flow strength, exhibiting a remarkable level of adaptability beyond surface texture alone. The experiments showed a relationship between the structure of the armor layer and Shields stress (shear stress corrected by D50) alongside the composition of the main channel bed (parent bed). This highlights the significance of flow strength and the underlying bed composition in shaping the formation and characteristics of the armor layer.

Berni et al. [33] conducted a study to explore the relationship between equilibrium time and sediment rate during the formation of the armor layer. Four key parameters that influence this relationship were identified, namely Reynolds number, non-dimensional median grain diameter, the ratio of channel bed shear stress to critical shear stress, and the ratio of width to flow depth. Laboratory datasets were collected under steady flow conditions to examine sediment transport rates without its supply from upstream. The analyses of these datasets aimed to gain insights into the factors contributing to the reduction of sediment rate during the armor layer formation process and its implications on the equilibrium time.

1.3. Shear Stress

The average shear stress is a critical parameter for predicting sediment transport, slope stability, and other aspects of river engineering in natural flow [34]. When describing flow in open channels and natural rivers, simplified one-dimensional hydraulic equations are often used to analyze cross-sections. According to Te Chow [35] and Graf and Altinakar [27], the velocity at all cross-sectional points remains constant in the case of uniform flow. Therefore, the forces acting on the system are in equilibrium (ΣF=0), as shown in Figure 3. In this context, the frictional force (F_f) is generated by the wall shear stress (τ0) acting on the wetted area Pdx, where P represents the wetted perimeter, as shown in Equation 3.

$$F_f = \tau_0 P dx \tag{3}$$

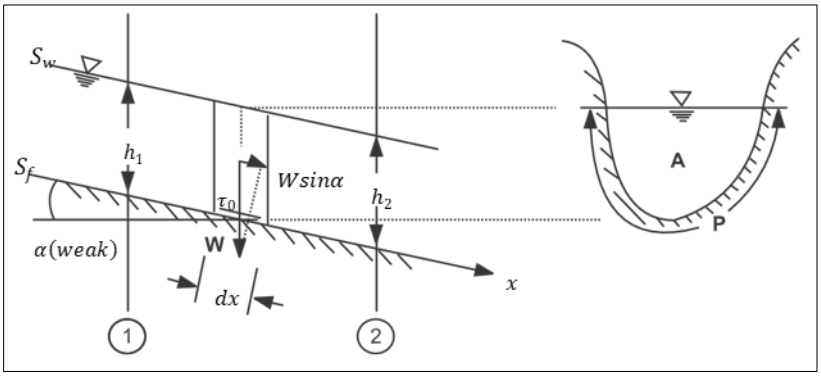

Figure 3. Uniform Flow Scheme [24]

The gravitational force is γAdx, where γ denotes the density of water, and the force acts in the flow direction, as shown in Equation 4.

$$F_G = \gamma A dx \, sin\alpha = W sin\alpha \tag{4}$$

The force equilibrium is expressed in uniform flow, as shown in Equation 5.

$$\tau_0 P dx = \gamma A dx \, sin\alpha \tag{5}$$

$$\tau_0 = \gamma \frac{A}{P} sin\alpha \tag{6}$$

$$\tau_0 = \gamma R S_f \tag{7}$$

$$-\gamma A \Delta h - \tau_0 P dx = \rho A v \frac{dv}{dx} \Delta x \tag{8}$$

$$\tau_0 = -\gamma R \left(\frac{dh}{dx} + \frac{v}{g} \frac{dv}{dx} \right) \tag{9}$$

$$\tau_0 = -\gamma R \frac{d}{dx} \left(h + \frac{v^2}{2g} \right) \tag{10}$$

$$\tau_0 = \gamma R S_f \tag{11}$$

where S_f is the slope of the total energy line, also known as the energy or friction slope. According to Graf & Altinakar [27], hydrodynamics is defined as follows:

$$\frac{\tau_0}{\rho} = u_*^2 \tag{12}$$

where u_* is shear velocity, leading to Equation 13.

$$u_* = \sqrt{g \, R_h \, S_f} \tag{13}$$

1.4. Critical Shear Stress

Erosion on the channel bed occurs when beds shear stress (τ_0^*) exceeds the critical shear stress (τ_{cr}^*)[27]. The resistance of grain to motion varies depending on their size, relative size to the surrounding grain, as well as their

orientation and depth within the bed. The weight of grain is influenced by its size, while the force required to roll grain along the channel bed is affected by its orientation. Additionally, the cohesion between grains impacts the magnitude of stress experienced by the affected grain.

In river hydraulics, the value of τ_{cr}^{*} can be calculated through the dimensionless shear stress parameter (τ^{*}), as shown in the Shields diagram in Figure 4.

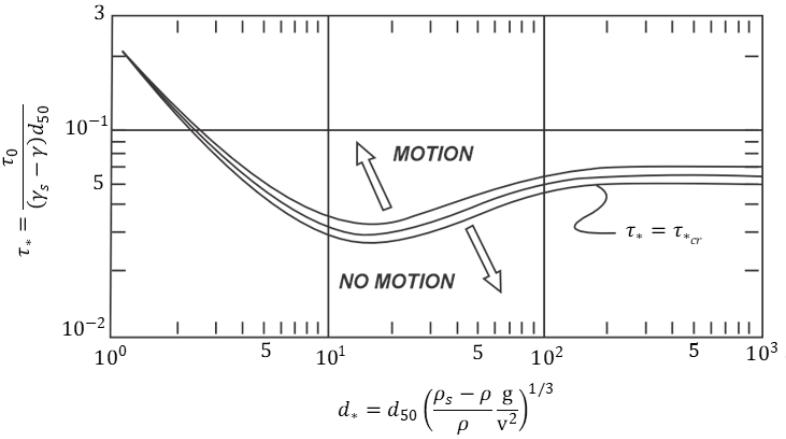

Figure 4. Relationship between (τ^{*}) with (d_{*}), Shield & Yalin [27]

The dimensionless grain diameter (d_{*}), dimensionless shear stress (τ_{*}) and critical shear stress on the channel bed (τ_{0cr}) are calculated as follows:

$$\tau_* = \frac{\tau_0}{(\gamma_s - \gamma)d_{50}} \approx \tau_{*cr} \quad (14)$$

$$\tau_{0cr} = \tau_{*cr}\, g(\rho_s - \rho)d_{50} \quad (15)$$

2. Materials and Methods

2.1. Experimental Set-up

This armor study is a laboratory experiment in hydraulics. It used a rectangular flume with channel walls made of plexiglass, specifically designed to examine different sediment transport phenomena under conditions of free surface flow and with the ability to vary bed slopes. The bed slope can be adjusted within certain limits, as shown in Figure 5.

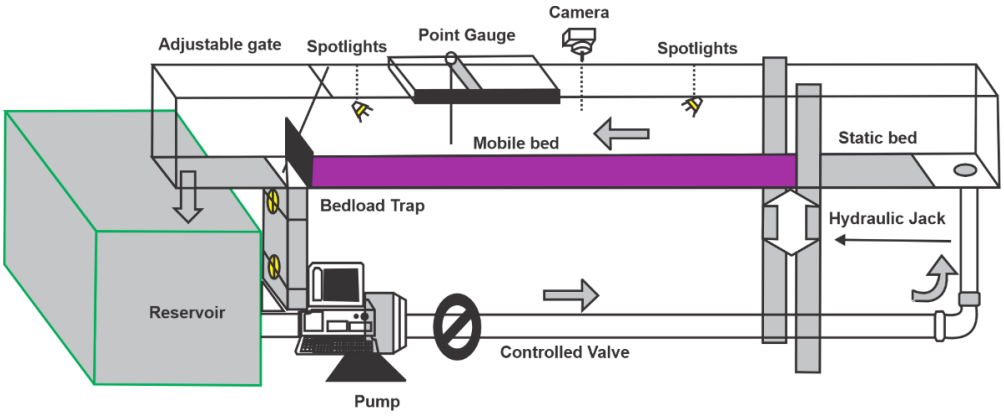

Figure 5. Installation of the Rectangular Flume

The rectangular flume had dimensions of 0.60, 10, and 0.45 m in width, length, and height, respectively, with walls made of plexiglass. The channel model was designed under free surface flow conditions with various slope variations. The channel bed slope (So) was adjusted according to the experimental plan. Beds slope limits in this study are 1, 1.4, 1.8, 2.2, and 2.6%, which were directly controlled using the limit switch indicated on the jacking post. Flow rate control was achieved by rotating the pump valve on the control panel. Flow circulation in the channel was controlled by a secondary circulation pump with a maximum flow rate capacity of 50 l/s. This study used a constant flow rate of 25 l/s, 30 l/s, 40 l/s, and 45 l/s. The installation of the rectangular flume can be seen in Figure 6.

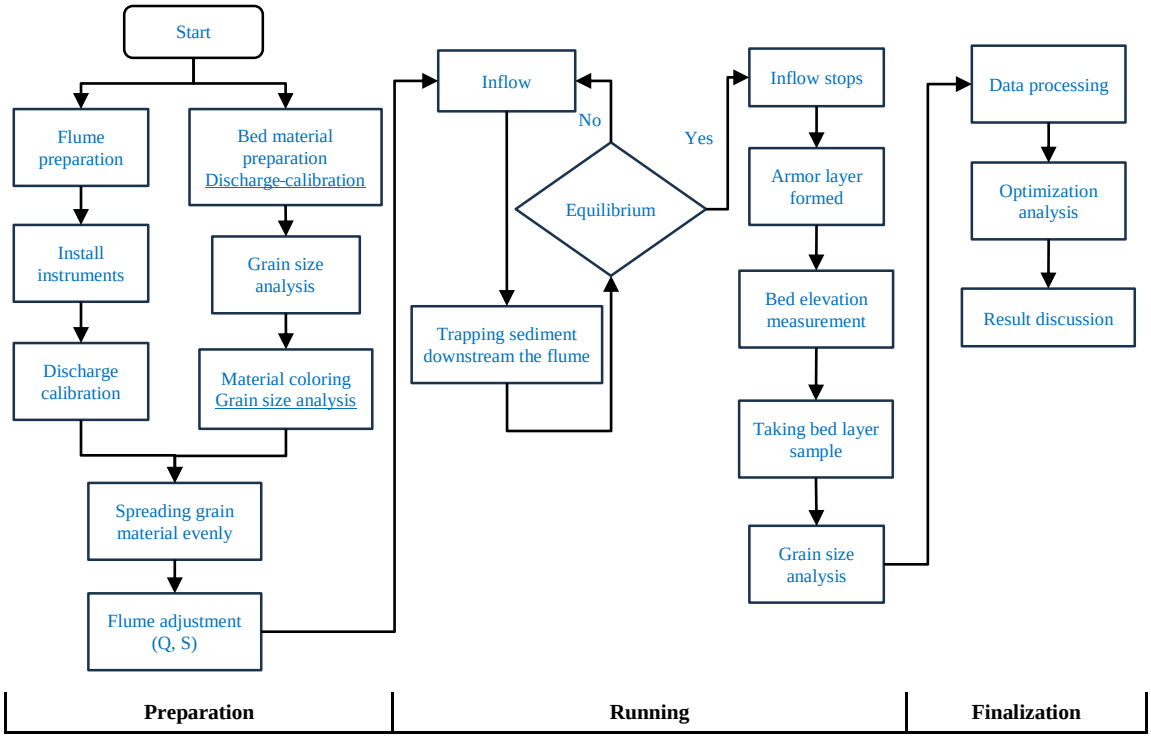

Figure 6. Workflow of laboratory experiments

Overall, the experiment consists of three stages, namely preparation, execution (running), and finalization (Figure 6). In each execution, there are two phases, including surface erosion and equilibrium. The experiment involved steady uniform flow, with variations in four different flow rates, five different materials gradations, and five different bed slope settings, culminating in 100 experimental runs. The workflow of the experiment is briefly shown in Figure 6.

At the beginning of the experiment, gravel, and sand sediments were evenly mixed along the channel with a material thickness boundary of 15 cm from the bottom. Additionally, water was discharged into the channel at a predetermined constant flow rate, corresponding to the set bed slope.

Data collection for the experiment started immediately after a steady uniform flow condition was achieved, where flow depth remained constant along the channel at a fixed discharge rate. In each experimental run, periodic measurements were conducted, including flow velocity, water temperature, water level, and the quantity of transported sediment. Flow velocity measurements were taken by installing a current meter at three vertical points in the middle of the channel, namely 0.4h, 0.6h, and 0.8h. Additionally, measurements of flow depth and collection of transported bedload grain were collected for analysis. The experiment continued until no bedload grain was transported out of the channel, after which flow discharge was stopped.

During the final stage of each experimental run, bedload grain collected in the sediment traps and any remaining gravel in the channel are gathered. The collected sediment was subjected to sieve analysis to determine the distribution of grain gradation.

2.2. Experimental Procedure

During the experiment, the gravel materials were segregated based on the diameter of grain size, with each fraction assigned a distinct color. The gravel grain size is specified using the D_{30}, D_{50}, D_{80}, and D_{90} values and is represented by the colors yellow, green, red, and white, respectively, dealing with their grain size. This study used five materials with different average grain size (D_{50}), including M_1=57, M_2=19, M_3=34, M_4=10, and M_5=51 mm.

Various measurements and calculations were performed for each experimental run, including analyzing the Froude number (F_r) and bed shear stress values for each discharge variation and channel bed slope. The analytical results obtained from these measurements and calculations are shown in Table 1.

Table 1. Analysis of Froude number and bed shear stress

Running	Q (l/s)	S	U (m/s)	h (m)	Fr	τ_o (N/m^2)	Running	Q (l/s)	S	U (m/s)	h (m)	Fr	τ_o (N/m^2)
M1Q1S1	25	0.010	0.53	0.080	0.597	7.85	M1Q3S1	40	0.010	0.62	0.110	0.598	10.79
M1Q1S2	25	0.014	0.60	0.070	0.705	9.61	M1Q3S2	40	0.014	0,70	0.100	0.708	13.73
M1Q1S3	25	0.018	0.66	0.065	0.797	11.48	M1Q3S3	40	0.018	0.75	0.090	0.802	15.89
M1Q1S4	25	0.022	0.70	0.066	0.878	12.95	M1Q3S4	40	0.022	0.81	0.085	0.886	18.34
M1Q1S5	25	0.026	0.73	0.067	0.951	14.03	M1Q3S5	40	0.026	0.85	0.080	0.962	20.40
M1Q2S1	30	0.010	0.56	0.090	0.598	8.83	M1Q4S1	45	0.010	0.65	0.120	0.597	11.77
M1Q2S2	30	0.014	0.63	0.080	0.706	10.99	M1Q4S2	45	0.014	0.74	0.110	0.708	15.11
M1Q2S3	30	0.018	0.69	0.075	0.799	13.24	M1Q4S3	45	0.018	0.80	0.100	0.803	17.66
M1Q2S4	30	0.022	0.73	0.070	0.881	15.11	M1Q4S4	45	0.022	0.83	0.090	0.887	19.42
M1Q2S5	30	0.026	0.76	0.065	0.955	16.58	M1Q4S5	45	0.026	0.91	0.085	0.964	21.68

3. Results and Discussion

3.1. Experimental Results

The critical bedload grain shear stress represents the minimum magnitude of bed shear stress required to initiate the motion of the bedload grain. In this study, the data for critical grain shear stress were obtained from the transported bedload grain in each experimental run, considering all materials (M_1, M_2, M_3, M_4, M_5), discharge (Q_1, Q_2, Q_3, Q_4), and bed slope (S_1, S_2, S_3, S_4, S_5) variations. The distribution of sediment discharge with corresponding bed shear stress values for each run-in flume for the five materials, four discharge, and five-bed slope variations is shown in Table 2.

Table 2. Measurement results of bed shear stress for M_1

Running	Q (l/s)	S	τ_o (N/m^2)	Qs (gr/s)	Running	Q (l/s)	S	τ_o (N/m^2)	Qs (gr/s)
M1Q1S1	25	0.010	7.85	26.66	M1Q3S1	40	0.101	10.79	36.65
M1Q1S2	25	0.014	9.61	61.51	M1Q3S2	40	0.014	13.73	87.88
M1Q1S3	25	0.018	11.48	82.02	M1Q3S3	40	0.018	15.89	113.56
M1Q1S4	25	0.022	12.95	125.08	M1Q3S4	40	0.022	18.34	177.20
M1Q1S5	25	0.026	14.03	205.05	M1Q3S5	40	0.026	20.40	298.25
M1Q2S1	30	0.010	8.83	29.99	M1Q4S1	45	0.010	11.77	39.98
M1Q2S2	30	0.014	10.99	70.30	M1Q4S2	45	0.014	15.11	96.67
M1Q2S3	30	0.018	13.24	94.64	M1Q4S3	45	0.018	17.66	126.18
M1Q2S4	30	0.022	15.11	145.93	M1Q4S4	45	0.022	19.42	187.62
M1Q2S5	30	0.026	16.58	242.33	M1Q4S5	45	0.026	21.68	316.98

Based on the data presented in Table 2, an illustration of the relationship between transported sediment discharge and bed shear stress is depicted in Figure 7. It shows the relationship between discharge variation and all bed slope variations. Based on Figure 7, the movement of bedload sediment grain occurred at a shear stress of 3.0 N/m^2, specifically at Q_s 0.3 gr/s, while grain started to move at a critical shear stress of 2.7 N/m^2.

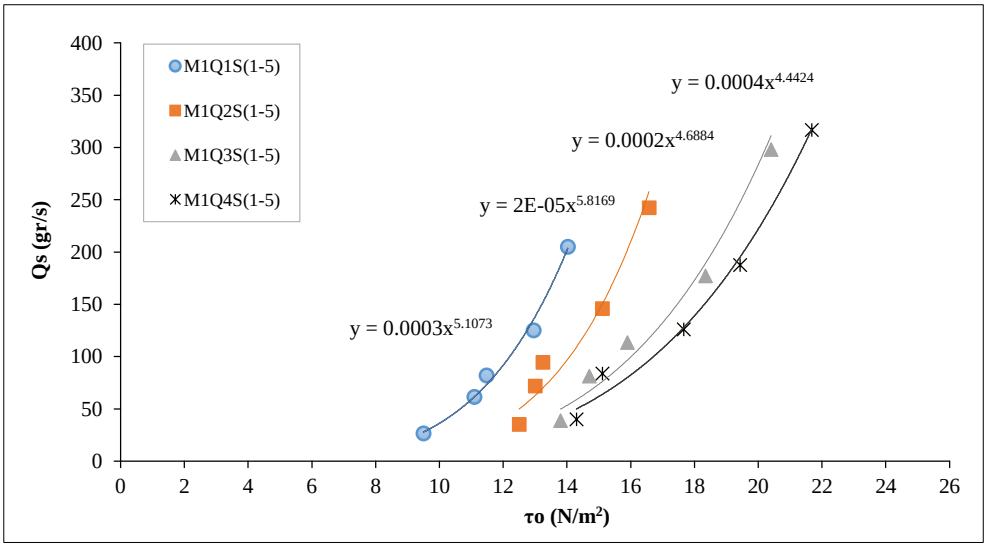

Figure 7. Rrelationship between Qs and τ_o for M_1

The relationship between bed shear stress and transported sediment discharge for all materials is shown in Figures 7 to 10.

- Figure 7 shows that the movement of bedload sediment grain occurs at a critical shear stress of 0.96 N/m^2, with a maximum value of 1.2 N/m^2.
- Figure 8 shows that shear stress reaches 1.4 N/m^2 with a transported sediment discharge of 0.2 gr/s, indicating a critical shear stress of 1.35 N/m^2.
- Figure 9 showed that the movement of sediment grain occurred at shear stress of 0.65 N/m^2 with a discharge of 0.1 gr/s, thereby indicating a critical shear stress of 0.61 N/m^2.
- Figure 10 shows the movement of bedload sediment grain at shear stress of 2.55 N/m^2, while the critical shear stress is 2.05 N/m^2

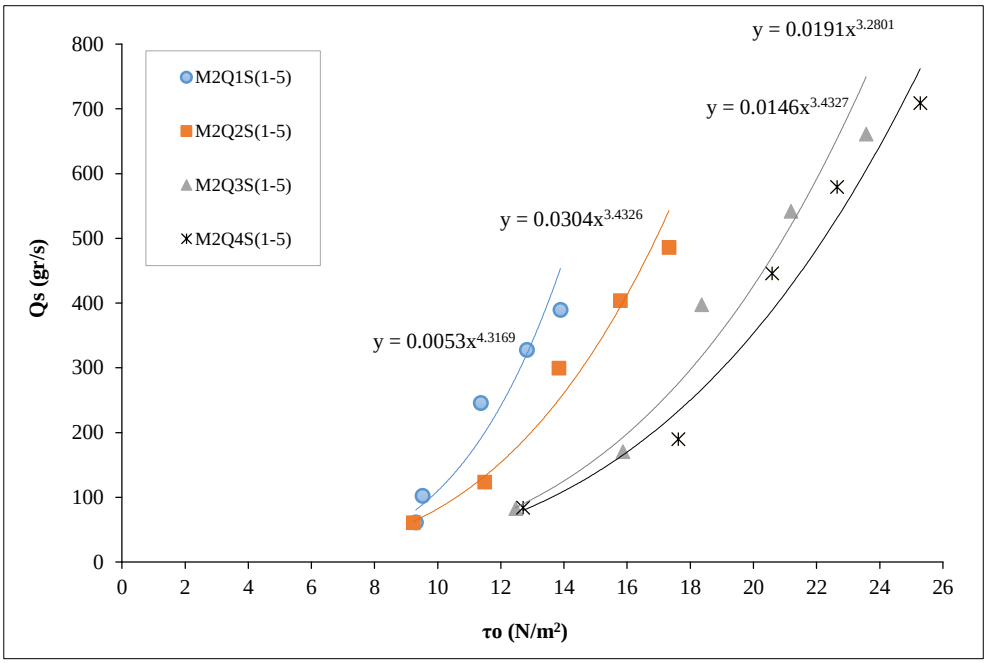

Figure 8. Relationship between Qs and τ_o for M_2

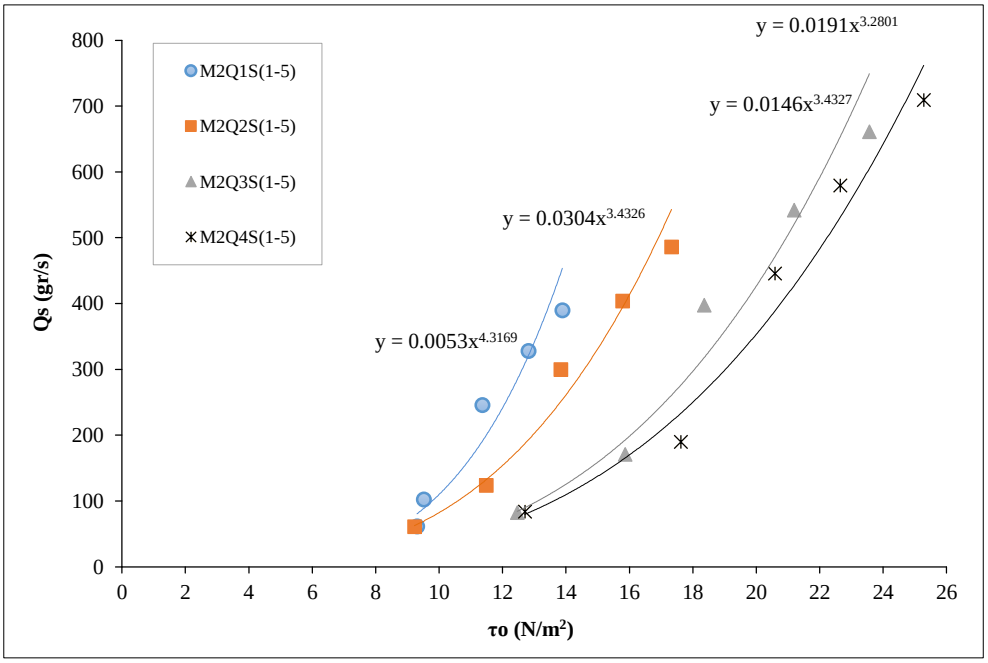

Figure 9. Relationship between Qs and τ_o for M_2

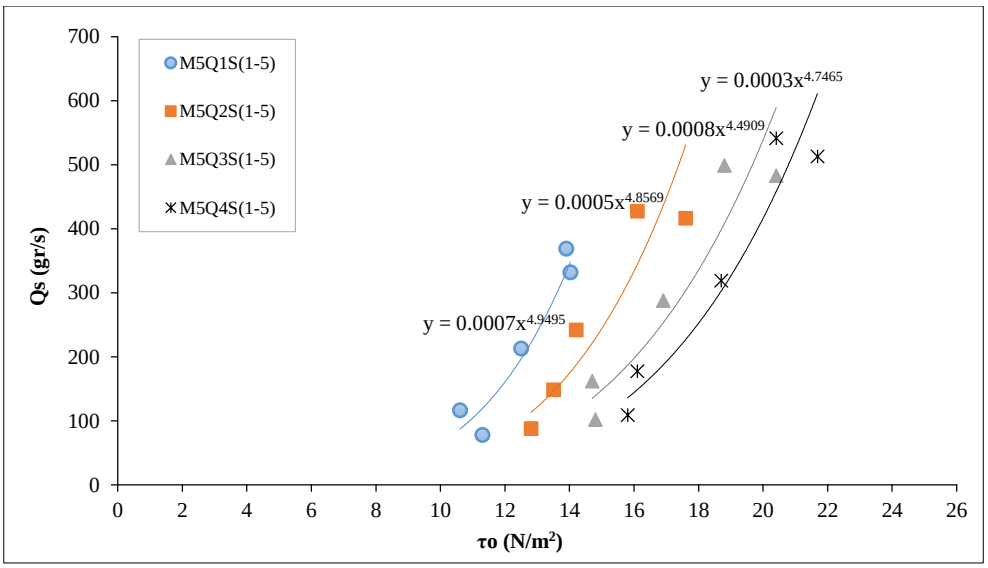

Figure 10. Relationship between Qs and τ_o for M_5

From the graph in Figure 11, four regression equations were derived to obtain the average critical bed shear stress value when the sediment discharge (Qs) was zero, as shown in Figure 12.

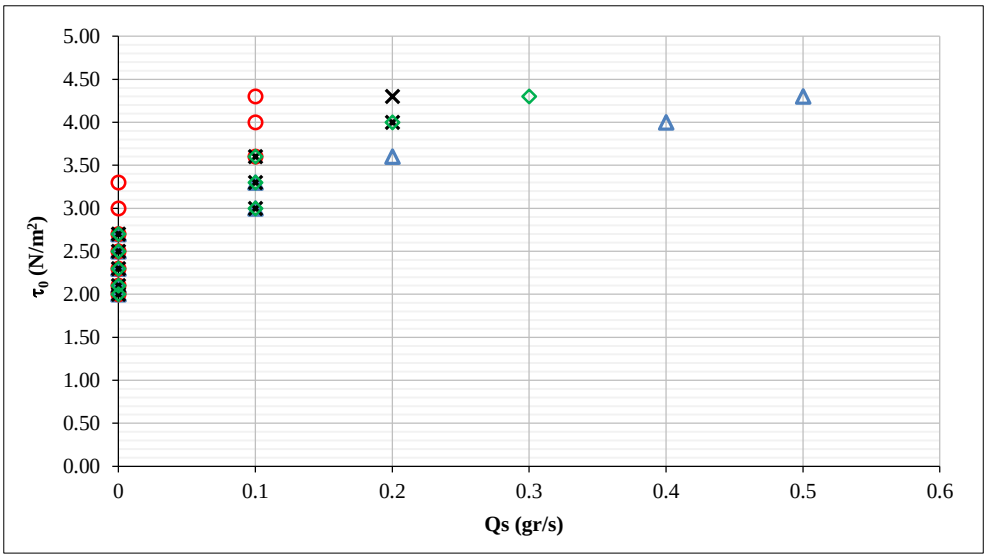

Figure 11. Analysis of shear stress for regression M_1

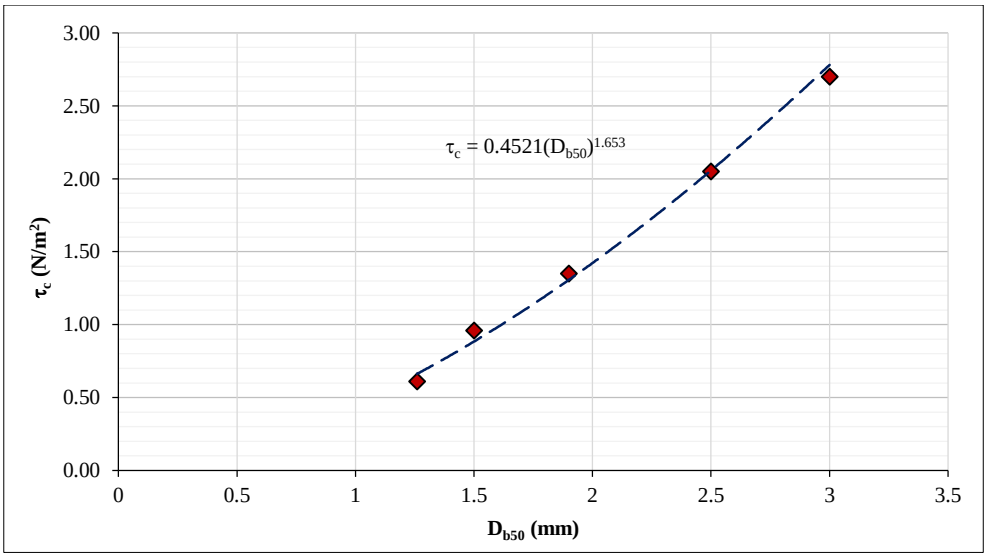

Figure 12. Critical grain shear stress (τ_c) corresponds to median grain diameter (D_{b50})

Overall, the critical grain shear stress in Figure 12 explained the relationship between τ_c and D_{b50} for all materials. It can be seen that the critical shear stress consistently rises in line with the grain size D_{b50}. Therefore, it can be understood that the larger the grain size, the greater the shear stress required to move the grain.

3.2. Discussion

3.2.1. Armor Layer Thickness (L_a)

Armor layer thickness is a dimensionless parameter defined as follows:

$$L_a = \left(\frac{D_{a50}}{D_{b50}}\right) \quad (16)$$

D_b represented the transported bedload grain captured in sediment traps during each run and subjected to sieve analysis, while Da_{50} is the remaining armor layer at the channel bed.

During the experiment, armor layer grain was collected using a specific method. Grain located at the top surface, which consisted of gravel and sand, was selected along a transverse direction of 50 cm. The sampling was performed horizontally across the channel width and vertically from the surface down to the bottom limit of the armor layer grain. The sampling technique followed the Wolman Pebble Count method developed by Wolman in 1954. This method involves sampling armor grain from the surface to the depth of the layer that still influences the above grain. The substrate layer sampling was also performed beneath the armor layer, followed by sieve analysis to determine grain size distribution. The following are the sieve analysis results of the transported bedload grain during the M1Q1S4 running, with D_{b50} and D_{a50} measuring 2.50mm and 63.00 mm, respectively.

$$L_a = \frac{D_{a50}}{D_{b50}} = \frac{63}{2.5} = 25.2 \quad (17)$$

3.2.2. Grain Uniformity Coefficient

The coefficient of uniformity (Cu) is an important parameter in sediment classification according to the Unified Soil Classification System (USCS). It quantifies grain diameter size observed in grain gradation analysis. A higher Cu value suggests a wider grain gradation range, indicating diverse and well-graded sediment grain size. Conversely, a smaller Cu value or Cu < 4 indicated an increasingly uniform size. The coefficient of uniformity according to the USCS is formulated as follows:

$$C_u = \frac{D_{60}}{D_{10}} \quad (18)$$

The value of Cu with the ratio of D60 to D10 was often used for grading fill materials.

In experiments involving natural or riverbed materials, the coefficient of uniformity (Cu), according to Limerinos (1970), was determined using the following formula:

$$C_u = \frac{D_{84}}{D_{16}} \quad (19)$$

In the experiment, the obtained C_u values decreased as the channel slope became steeper, with an increase in bed roughness. Meyer-Peter, Muler and Parker examined the value of bed roughness based on the protective layer approach. For D_{90}, the coefficient of uniformity can be calculated as follows:

$$Cu = \frac{D_{a90}}{D_{a16}} \quad (20)$$

The following are the sieve analysis results of the transported bedload grain during the M1Q1S4 running, with Da90 and Da16 measuring 90 mm and 35 mm, respectively.

The value of $C_u = \frac{D_{a90}}{D_{a16}}$ is $C_u = \frac{90}{35} = 2.571$.

3.2.3. Armor Layer Formula

Based on the experimental results, it is clear that armor layer formation started when beds shear stress exceeded the critical shear stress of the transported bedload grain. This led to the continuous movement of grain and resulted in surface erosion. Eventually, a stable condition was reached where no further bedload grain were transported. In this stable state, beds surface consisted predominantly of gravel and sand, with gravel dominating and exhibiting nearly uniform grain size. The parameters involved in the composition of armor layer are armor layer grain diameter (D_a), water density (ρ), shear stress difference ($\Delta\tau$), grain size uniformity (C_u), and flow velocity (U). These parameters are mathematically expressed in armor layer function as follows:

$$f(\rho, D_a, C_u, U, \Delta\tau) = 0 \quad (21)$$

Furthermore, dimensional analysis was performed using the Basic Stepwise Method. The SI units for the parameters in the function are water density (ML^{-3}), armor grain diameter (L), grain size uniformity (L/L), flow velocity (LT^{-1}), and shear stress difference ($ML^{-1}T^{-2}$).

The function is then transformed into dimensionless numbers:

$$f\left(\frac{D_a}{D_b}, \frac{(\Delta\tau)}{\tau}, C_u\right) = 0 \quad (22)$$

or;

$$f\left(\frac{D_{a50}}{D_{b50}}, \frac{(\tau_0-\tau_c)}{\tau_c}, C_u\right) = 0 \quad (23)$$

or

$$\frac{D_{a50}}{D_{b50}} = f\left(\frac{(\tau_o-\tau_c)}{\tau_c}, C_u\right) \quad (24)$$

In these equations, three dimensionless components interact in armor layer mechanism, including $\frac{D_{a50}}{D_{b50}}$, $\frac{(\tau_o-\tau_c)}{\tau_c}$ and $C_u = \frac{D_{a90}}{D_{a16}}$, denoting thickness of the protective layer, beds shear stress difference and grain size uniformity. Beds shear stress component needs to be always positive. Therefore, the equation is modified by introducing a value of θ to ensure shear stress graph remains positive. For grain size uniformity, a modification was made by introducing a value of λ to ensure a minimum value of unity for grain size uniformity. The equation became:

$$\frac{D_{a50}}{D_{b50}} = \left(\frac{\tau_o-\tau_c}{\tau_c} - \theta\right)\left(C_u - \lambda\right) \quad (25)$$

Moreover, the equation underwent multiplication of $\alpha$and raised to the power of $\beta$for shear stress component, while grain size uniformity was raised to the power of γ. Therefore, the equation became:

$$\frac{D_{a50}}{D_{b50}} = \alpha\left(\frac{\tau_o-\tau_c}{\tau_c} - \theta\right)^{\beta}\left(C_u - \lambda\right)^{\gamma} \quad (26)$$

The coefficient of $\alpha, \beta, \gamma, \theta, \lambda$ was obtained through optimization analysis of 100 data points derived from the runs of 5 experimental materials, using an Excel spreadsheet in the x-y coordinate system. The optimization analysis is considered valid, assuming the sum of the values$\sqrt{opt}$ is divided by the number of data points, raised to the power of 0.5, and approaches 0. In this optimization analysis, the value of 1.63 was obtained, as shown in Table 4.

Table 3. Experimental analysis results of M_1, with τ_c = 2.70 N/m^2

Running	Q (1/s)	S	U (m/s)	h (m)	Fr	τ_0 (N/m^2)	U (m/s)	D_{a90} (mm)	D_{a16} (mm)	C_u	D_{a50} (mm)	D_{b50} (mm)	$\frac{D_{a50}}{D_{b50}}$	$\frac{\tau_0-\tau_c}{\tau_c}$ (N/m^2)
M1Q1S1	25	0.010	0.53	0.080	0.597	7.85	0.09	84	35	2.40	61	2.9	21.00	1.91
M1Q1S2	25	0.014	0.60	0.070	0.705	9.61	0.10	86	35	2.46	61	2.7	22.50	2.56
M1Q1S3	25	0.018	0.66	0.067	0.797	11.48	0.11	89	36	2.47	60	2.5	24.00	3.25
M1Q1S4	25	0.022	0.70	0.066	0.878	12.95	0.11	90	35	2.57	63	2.5	25.00	3.80
M1Q1S5	25	0.026	0.73	0.065	0.951	14.03	0.12	91	34	2.68	60	2.3	26.00	4.20
M1Q2S1	30	0.010	0.56	0.090	0.598	8.83	0.09	85	35	2.43	60	3.6	15.72	2.27
M1Q2S2	30	0.014	0.63	0.080	0.706	10.99	0.10	88	35	2.51	62	3.4	18.17	3.07
M1Q2S3	30	0.018	0.69	0.075	0.799	13.24	0.12	89	35	2.54	60	2.1	19.41	3.91
M1Q2S4	30	0.022	0.73	0.070	0.811	15.11	0.12	90	34	2.65	59	2.3	22.52	4.60
M1Q2S5	30	0.026	0.76	0.065	0.955	16.58	0.13	92	33	2.79	63	2.6	24.21	5.14
M1Q3S1	40	0.010	0.62	0.100	0.598	10.79	0.10	86	35	2.46	62	3.5	17.69	3.00
M1Q3S2	40	0.014	0.70	0.100	0.708	13.73	0.12	89	34	2.62	63	3.3	19.10	4.09
M1Q3S3	40	0.018	0.75	0.090	0.802	15.89	0.13	90	32	2.81	61	2.7	22.55	4.89
M1Q3S4	40	0.022	0.81	0.085	0.886	18.34	0.14	91	31	2.94	59	2.5	23.43	5.79
M1Q3S5	40	0.026	0.85	0.080	0.962	20.40	0.14	93	31	3.00	61	2.4	25.43	6.56
M1Q4S1	50	0.010	0.65	0.120	0.597	11.77	0.11	87	34	2.56	61	3.3	17.76	3.36
M1Q4S2	50	0.014	0.74	0.110	0.708	15.11	0.12	89	33	2.70	61	3.0	20.31	4.60
M1Q4S3	50	0.018	0.80	0.100	0.803	17.66	0.13	90	32	2.81	61	2.8	21.89	5.54
M1Q4S4	50	0.022	0.83	0.090	0.887	19.42	0.14	93	30	3.10	61	2.7	22.43	6.19
M1Q4S5	50	0.026	0.91	0.085	0.964	21.68	0.15	93	28	3.32	61	2.7	22.70	7.03

Table 4. Optimization analysis results

No. Run	$\frac{D_{a50}}{D_{b50}}$	$\frac{\tau_0-\tau_c}{\tau_c}$	$\frac{\tau_0-\tau_c}{\tau_c}-\theta$	C_u	$(C_u-\lambda)$	$\left(\frac{\tau_0-\tau_c}{\tau_c}-\theta\right)(C_u-\lambda)$	$E=\frac{D_{a50}}{D_{b50}}-\alpha\left(\frac{\tau_0-\tau_c}{\tau_c}-\theta\right)^{\beta}(C_u-\lambda)^{\gamma}$	E^2	Optimasi	$\sqrt{opt}$
1	21.0	1.91	0.91	2.46	1.46	1.32	19.68	387.16	37.26	6.10
2	22.5	2.61	1.61	2.46	1.46	2.35	20.15	406.09	24.13	4.91
3	24.0	3.32	2.32	2.47	1.47	3.41	20.59	423.94	17.01	4.12
4	25.0	3.88	2.88	2.57	1.57	4.52	20.48	419.46	11.73	3.42
5	26.0	4.48	3.48	2.68	1.68	5.83	20.17	406.73	7.46	2.73
6	16.7	2.27	1.27	2.46	1.46	1.85	14.87	221.12	0.14	0.37
7	18.2	3.07	2.07	2.51	1.51	3.13	15.04	226.17	0.96	0.98
8	19.4	3.84	2.84	2.54	1.54	4.38	15.03	225.98	4.14	2.04
9	22.5	4.52	3.52	2.65	1.65	5.79	16.73	279.80	0.67	0.82
10	24.2	5.14	4.14	2.79	1.79	7.40	16.80	282.39	0.62	0.79
11	17.7	2.92	1.92	2.46	1.46	2.80	14.89	221.60	0.90	0.95
12	19.1	3.88	2.88	2.62	1.62	4.66	14.44	208.50	6.42	2.53
13	22.6	4.82	3.82	2.81	1.81	6.92	15.63	244.20	2.88	1.70
14	23.4	5.63	4.63	2.94	1.94	8.97	14.46	209.05	8.11	2.85
15	25.4	6.46	5.46	2.87	1.87	10.22	15.21	231.44	6.61	2.57
16	17.8	3.25	2.25	2.56	1.56	3.51	14.25	203.05	3.97	1.99
17	20.3	4.29	3.29	2.70	1.70	5.58	14.73	216.89	6.20	2.49
18	21.9	5.28	4.28	2.81	1.81	7.75	14.14	199.86	11.90	3.45
19	22.4	6.19	5.19	3.10	2.10	10.91	11.53	132.83	27.35	5.23
20	22.7	7.03	6.03	3.32	2.32	14.00	8.71	75.78	47.67	6.90
21	36.0	7.18	6.18	3.69	2.69	16.63	19.38	375.39	33.23	5.76
22	38.0	9.16	8.16	3.50	2.50	20.39	17.61	309.99	18.02	4.24
23	40.0	11.14	10.14	3.71	2.71	27.52	12.48	155.69	7.55	2.75
24	42.0	12.71	11.71	3.53	2.53	29.67	12.33	151.92	6.63	2.57
25	44.0	14.41	13.41	3.67	2.67	35.76	8.24	67.90	4.14	2.03
26	36.7	8.20	7.20	4.55	3.55	25.52	11.15	124.33	14.01	3.74
27	38.3	10.45	9.45	5.00	4.00	37.78	0.55	0.31	1.10	1.05
28	40.8	12.61	11.61	4.83	3.83	44.51	-3.68	13.52	0.06	0.24
29	42.5	14.51	13.51	4.62	3.62	48.85	-6.35	40.34	0.40	0.64
30	45.0	16.27	15.27	4.50	3.50	53.44	-8.44	71.30	0.14	0.38
31	37.9	10.04	9.04	5.00	4.00	36.15	1.71	2.93	1.60	1.26
32	40.7	12.73	11.73	5.25	4.25	49.87	-9.16	83.82	0.17	0.41
33	42.1	15.37	14.37	4.64	3.64	52.35	-10.21	104.17	4.80	2.19
34	45.7	17.66	16.66	4.71	3.71	61.88	-16.16	261.26	2.74	1.66
35	45.7	19.99	18.99	4.25	3.25	61.72	-16.00	256.03	15.37	3.92
36	38.1	10.96	9.96	5.00	4.00	39.82	-1.70	2.89	0.00	0.01
37	38.8	13.88	12.88	4.40	3.40	43.79	-5.04	25.37	10.79	3.29
38	39.4	16.66	15.66	4.19	3.19	49.91	-10.53	110.98	37.91	6.16
39	41.9	19.23	18.23	4.38	3.38	61.54	-19.66	386.59	49.39	7.03
40	43.1	21.58	20.58	4.29	3.29	67.80	-24.68	609.07	69.94	8.36
41	26.7	4.06	3.06	6.09	5.09	15.59	11.07	122.59	6.14	2.48
42	27.3	5.29	4.29	5.75	4.75	20.38	6.95	48.31	0.00	0.02
43	29.3	6.52	5.52	5.92	4.92	27.13	2.20	4.83	1.01	1.01
44	30.7	7.49	6.49	5.62	4.62	29.97	0.70	0.48	2.51	1.59
45	32.7	8.54	7.54	5.36	4.36	32.87	-0.20	0.04	2.22	1.49
46	27.1	4.70	3.70	5.23	4.23	15.64	11.42	130.45	2.24	1.50
47	28.2	6.09	5.09	5.00	4.00	20.35	7.88	62.11	0.38	0.62
48	30.6	7.43	6.43	5.21	4.21	27.10	3.49	12.17	1.66	1.29
49	30.6	8.61	7.61	5.00	4.00	30.43	0.16	0.03	11.86	3.44
50	32.9	9.70	8.70	5.07	4.07	35.36	-2.42	5.87	9.68	3.11

No. Run	$\frac{D_{a50}}{D_{b50}}$	$\frac{\tau_0-\tau_c}{\tau_c}$	$\frac{\tau_0-\tau_c}{\tau_c}-\theta$	C_u	$(C_u-\lambda)$	$\left(\frac{\tau_0-\tau_c}{\tau_c}-\theta\right)(C_u-\lambda)$	$E=\frac{D_{a50}}{D_{b50}}-\alpha\left(\frac{\tau_0-\tau_c}{\tau_c}-\theta\right)^{\beta}(C_u-\lambda)^{\gamma}$	E^2	Optimasi	$\sqrt{opt}$
51	28.4	5.84	4.84	5.21	4.21	20.38	8.04	64.70	0.00	0.03
52	30.0	7.51	6.51	5.00	4.00	26.02	3.98	15.80	3.58	1.89
53	31.1	9.14	8.14	5.13	4.13	33.64	-2.59	6.70	16.44	4.05
54	33.7	10.56	9.56	4.81	3.81	36.44	-2.75	7.57	13.25	3.64
55	33.7	12.00	11.00	4.59	3.59	39.47	-5.79	33.48	33.15	5.76
56	30.0	6.40	5.40	4.69	3.69	19.93	10.07	101.39	0.40	0.64
57	31.4	8.22	7.22	4.75	3.75	27.06	4.37	19.11	2.83	1.68
58	32.4	9.94	8.94	4.53	3.53	31.54	0.84	0.71	13.44	3.67
59	34.3	11.53	10.53	4.59	3.59	37.79	-3.50	12.28	19.60	4.43
60	35.2	12.99	11.99	4.44	3.44	41.29	-6.05	36.61	30.86	5.56
61	48.2	11.87	10.87	3.00	2.00	21.73	26.47	700.60	114.26	10.69
62	49.7	14.99	13.99	3.13	2.13	29.72	19.98	399.23	58.98	7.68
63	51.6	18.11	17.11	3.13	2.13	36.35	15.25	232.60	32.64	5.71
64	53.6	20.58	19.58	3.00	2.00	39.16	14.44	208.40	26.12	5.11
65	54.5	23.25	22.25	3.00	2.00	44.50	10.00	99.94	10.19	3.19
66	49.3	13.47	12.47	3.57	2.57	32.08	17.22	296.69	76.45	8.74
67	50.9	17.01	16.01	3.25	2.25	36.03	14.87	221.22	37.65	6.14
68	52.8	20.42	19.42	3.38	2.38	46.13	6.67	44.55	15.02	3.88
69	54.9	23.41	22.41	3.00	2.00	44.82	10.08	101.51	11.75	3.43
70	56.1	26.18	25.18	3.20	2.20	55.39	0.71	0.50	2.32	1.52
71	49.9	16.37	15.37	3.63	2.63	40.34	9.56	91.35	29.37	5.42
72	52.3	20.61	19.61	3.88	2.88	56.39	-4.09	16.73	5.95	2.44
73	55.3	24.76	23.76	3.88	2.88	68.32	-13.02	169.51	1.04	1.02
74	56.3	28.37	27.37	3.20	2.20	60.20	-3.90	15.24	0.11	0.34
75	57.2	32.03	31.03	3.09	2.09	64.89	-7.69	59.07	6.18	2.49
76	50.1	17.82	16.82	3.20	2.20	36.99	13.11	171.74	19.71	4.44
77	54.1	22.42	21.42	4.13	3.13	66.92	-12.82	164.43	3.69	1.92
78	55.9	26.79	25.79	3.40	2.40	61.90	-6.00	35.94	0.15	0.38
79	56.9	30.84	29.84	3.50	2.50	74.61	-17.71	313.49	6.42	2.53
80	57.5	34.54	33.54	3.17	2.17	72.67	-15.17	230.20	19.87	4.46
81	21.0	2.90	1.90	4.71	3.71	7.06	13.94	194.39	1.20	1.10
82	23.0	3.85	2.85	4.50	3.50	9.98	13.02	169.53	0.03	0.17
83	24.5	4.80	3.80	4.32	3.32	12.59	11.91	141.76	0.67	0.82
84	26.0	5.55	4.55	4.37	3.37	15.33	10.67	113.94	1.45	1.21
85	27.5	6.36	5.36	4.15	3.15	16.88	10.62	112.70	1.94	1.39
86	22.4	3.39	2.39	4.05	3.05	7.30	15.08	227.52	1.41	1.19
87	23.3	4.47	3.47	3.86	2.86	9.90	13.43	180.36	0.68	0.83
88	25.7	5.50	4.50	3.73	2.73	12.28	13.44	180.61	0.86	0.93
89	29.0	6.41	5.41	3.61	2.61	14.11	14.94	223.14	0.22	0.47
90	31.9	7.25	6.25	3.23	2.23	13.94	17.97	322.79	3.80	1.95
91	23.0	4.27	3.27	3.61	2.61	8.53	14.51	210.55	0.18	0.43
92	25.2	5.56	4.56	3.46	2.46	11.21	14.01	196.24	1.82	1.35
93	29.6	6.82	5.82	3.36	2.36	13.73	15.83	250.69	0.12	0.35
94	34.3	7.91	6.91	3.27	2.27	15.68	18.66	348.31	9.48	3.08
95	34.8	9.02	8.02	3.07	2.07	16.62	18.16	329.78	2.97	1.72
96	25.0	4.71	3.71	3.27	2.27	8.42	16.58	274.91	0.40	0.63
97	26.7	6.11	5.11	3.27	2.27	11.59	15.08	227.40	0.93	0.96
98	30.8	7.43	6.43	3.19	2.19	14.06	16.77	281.39	0.32	0.56
99	33.3	8.66	7.66	3.22	2.22	17.03	16.30	265.79	0.55	0.74
100	34.2	9.79	8.79	3.14	2.14	18.83	15.34	235.29	0.07	0.27
										1.63

Meanwhile, the coefficients of $\alpha, \beta, \gamma, \theta, \lambda$ are:

α : 11.05;
β : 0.46;
γ : 0.10;
θ : 0.30;
λ : 0.20.

Therefore, the armor layer formula (La) is:

$$\frac{D_{a50}}{D_{b50}} = 11.05\left(\frac{\tau_o-\tau_c}{\tau_c} - 0.30\right)^{0.46}\left(C_u - 0.20\right)^{0.10} \quad (27)$$

In the optimization analysis, the average value of Cu is found to be 3.8. The relationship between armor layer thickness and non-dimensional shear stress is presented in Figure 12 as follows:

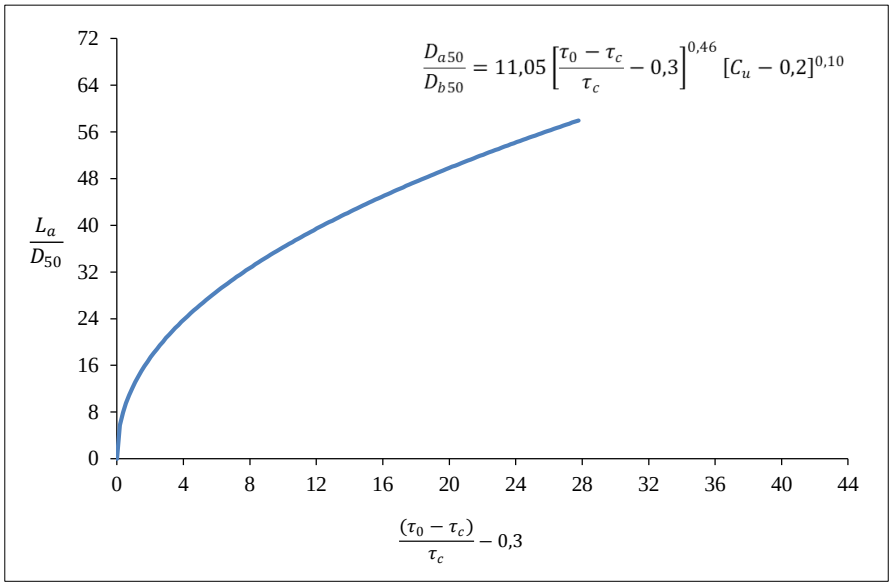

Figure 13. Graph of the Relationship between Armor Layer Thickness Ratio and Non-Dimensional Shear Stress

4. Conclusion

In conclusion, a series of laboratory experiments were conducted to examine the influence of shear stress and uniformity coefficient on grain size profile and armor layer thickness under steady uniform flow. The experiments involved varying four flow discharges, five-bed slopes, and five materials variations, resulting in 100 experimental runs. During the process of surface erosion, it was observed that the armor layer structure exhibited greater resilience on the surface. This phenomenon was attributed to the fact that shear stress exerted on armor grain exceeded bed shear stress. The uniformity coefficient (C_u) values tend to decrease as the slope of the channel becomes steeper in line with increasing layer roughness. As a result, armor grain consisted of sediment grain structures with a critical shear stress higher than bed shear stress. The formula for calculating armor layer thickness was expressed using dimensionless numbers, subject to specific constraints. These constraints included bedload diameter ranging from 0.8 mm to 2.9 mm, a uniformity coefficient 3.8, a critical shear stress ranging from 0.61 N/m^2 to 2.7 N/m^2, and a minimum bed shear stress of 6 N/m^2. Armor layer thickness corresponding to dimensionless shear stress was developed to estimate the degree of armoring that provides sufficient bed channel protection.

5. Declarations

5.1. Data Availability Statement

The data presented in this study are available in the article.

5.2. Funding and Acknowledgements

The author acknowledges the funding provided by LPPM Sebelas Maret University.

5.3. Conflicts of Interest

The author declares no conflict of interest.

6. References

[1] Hunziker, R. P., & Jaeggi, M. N. R. (2002). Grain Sorting Processes. Journal of Hydraulic Engineering, 128(12), 1060–1068. doi:10.1061/(asce)0733-9429(2002)128:12(1060).

[2] Vázquez-Tarrío, D., Piégay, H., & Menéndez-Duarte, R. (2020). Textural signatures of sediment supply in gravel-bed rivers: Revisiting the armour ratio. Earth-Science Reviews, 207. doi:10.1016/j.earscirev.2020.103211.

[3] Cooper, J. R., & Tait, S. J. (2009). Water-worked gravel beds in laboratory flumes - A natural analogue? Earth Surface Processes and Landforms, 34(3), 384–397. doi:10.1002/esp.1743.

[4] Yager, E. M., Kenworthy, M., & Monsalve, A. (2015). Taking the river inside: Fundamental advances from laboratory experiments in measuring and understanding bedload transport processes. Geomorphology, 244, 21–32. doi:10.1016/j.geomorph.2015.04.002.

[5] Recking, A. (2013). Simple Method for Calculating Reach-Averaged Bed-Load Transport. Journal of Hydraulic Engineering, 139(1), 70–75. doi:10.1061/(asce)hy.1943-7900.0000653.

[6] Heays, K. G., Friedrich, H., & Melville, B. W. (2014). Laboratory study of gravel-bed cluster formation and disintegration. Water Resources Research, 50(3), 2227–2241. doi:10.1002/2013WR014208.

[7] Ancey, C. (2020). Bedload transport: a walk between randomness and determinism. Part 1. The state of the art. Journal of Hydraulic Research, 58(1), 1–17. doi:10.1080/00221686.2019.1702594.

[8] Wang, L., Wang, D., Cuthbertson, A., Zhong, D., & Pender, G. (2021). Hysteretic Implications for Graded Bed Load Sediment Transport in Symmetrical Hydrograph Flows. Frontiers in Environmental Science, 9. doi:10.3389/fenvs.2021.800832.

[9] Mrokowska, M. M., & Rowinski, P. M. (2019). Impact of unsteady flow events on bedload transport: A review of laboratory experiments. Water (Switzerland), 11(5). doi:10.3390/w11050907.

[10] Negara, A. S., Ikhsan, C., Hadiani, Rr. R., & Purwana, Y. M. (2023). Effect of bed shear stress on the mobile armor layer at the riverbed. IOP Conference Series: Earth and Environmental Science, 1195(1), 012057. doi:10.1088/1755-1315/1195/1/012057.

[11] Chin, C. O., Melville, B. W., & Raudkivi, A. J. (1994). Streambed Armoring. Journal of Hydraulic Engineering, 120(8), 899–918. doi:10.1061/(asce)0733-9429(1994)120:8(899).

[12] Wilcock, P. R., & DeTemple, B. T. (2005). Persistence of armor layers in gravel-bed streams. Geophysical Research Letters, 32(8), 1–4. doi:10.1029/2004GL021772.

[13] Aberle, J., & Nikora, V. (2006). Statistical properties of armored gravel bed surfaces. Water Resources Research, 42(11), 1-11. doi:10.1029/2005WR004674.

[14] Zhang, S., Zhu, Z., Peng, J., He, L., & Chen, D. (2021). Laboratory study on the evolution of gravel-bed surfaces in bed armoring processes. Journal of Hydrology, 597. doi:10.1016/j.jhydrol.2020.125751.

[15] Marion, A., & Fraccarollo, L. (1997). Experimental investigation of mobile armoring development. Water Resources Research, 33(6), 1447–1453. doi:10.1029/97WR00705.

[16] Elgueta-Astaburuaga, M. A., & Hassan, M. A. (2019). Sediment storage, partial transport, and the evolution of an experimental gravel bed under changing sediment supply regimes. Geomorphology, 330, 1–12. doi:10.1016/j.geomorph.2018.12.018.

[17] Church, M., Hassan, M. A., & Wolcott, J. F. (1998). Stabilizing self-organized structures in gravel-bed stream channels: Field and experimental observations. Water Resources Research, 34(11), 3169–3179. doi:10.1029/98WR00484.

[18] Ikhsan, C., Rahajo, A., & Legono, D. (2014). The formation of static armour layer. International Journal of Civil & Environmental Engineering, 14, 19-23.

[19] Mao, L., Cooper, J. R., & Frostick, L. E. (2011). Grain size and topographical differences between static and mobile armour layers. Earth Surface Processes and Landforms, 36(10), 1321–1334. doi:10.1002/esp.2156.

[20] Spiller, S. M., Rüther, N., & Friedrich, H. (2015). Dynamic lift on an artificial static armor layer during highly unsteady open channel flow. Water (Switzerland), 7(9), 4951–4970. doi:10.3390/w7094951.

[21] Curran, J. C., & Waters, K. A. (2014). The importance of bed sediment sand content for the structure of a static armor layer in a gravel bed river. Journal of Geophysical Research: Earth Surface, 119(7), 1484–1497. doi:10.1002/2014JF003143.

[22] Ikhsan, C., Raharjo, A. P., Legono, D., & Kironoto, B. A. (2020). Effek Tegangan Geser dan Keseragaman Butiran terhadap Tebal Armour Layer pada Kondisi Statis di Dasar Saluran. Jurnal Teknik Sipil, 27(3), 247. doi:10.5614/jts.2020.27.3.6. (In Indonesian).

[23] Almedeij, J. H. (2002). Bedload transport in gravel-bed streams under a wide range of Shields stresses. Ph.D. Thesis, Virginia Tech, Blacksburg, United States.

[24] Powell, D. M., Ockelford, A., Rice, S. P., Hillier, J. K., Nguyen, T., Reid, I., Tate, N. J., & Ackerley, D. (2016). Structural properties of mobile armors formed at different flow strengths in gravel-bed rivers. Journal of Geophysical Research: Earth Surface, 121(8), 1494–1515. doi:10.1002/2015JF003794.

[25] Marion, A., Tait, S. J., & McEwan, I. K. (2003). Analysis of small-scale gravel bed topography during armoring. Water Resources Research, 39(12). doi:10.1029/2003WR002367.

[26] Wang, Q., Pan, Y., Yang, K., & Nie, R. (2020). Structural properties of the static armor during formation and reestablishment in gravel-bed rivers. Water (Switzerland), 12(7). doi:10.3390/w12071845.

[27] Graf, W. H., & Altinakar, M. S. (1998). Fluvial hydraulics: Flow and transport processes in channels of simple geometry. Wiley, New York, United States.

[28] 26-Lisle, T. E., & Madej, M. A. (1992). Spatial variation in armouring in a channel with high sediment supply. Dynamics of gravel-bed rivers, 277-293. John Wiley & Sons, Hoboken, United States.

[29] Wilcock, P. R., Kenworthy, S. T., & Crowe, J. C. (2001). Experimental study of the transport of mixed sand and gravel. Water Resources Research, 37(12), 3349–3358. doi:10.1029/2001WR000683.

[30] Vericat, D., Batalla, R. J., & Garcia, C. (2006). Breakup and reestablishment of the armour layer in a large gravel-bed river below dams: The lower Ebro. Geomorphology, 76(1–2), 122–136. doi:10.1016/j.geomorph.2005.10.005.

[31] Viparelli, E., Gaeuman, D., Wilcock, P., & Parker, G. (2011). A model to predict the evolution of a gravel bed river under an imposed cyclic hydrograph and its application to the Trinity River. Water Resources Research, 47(2), 1-22. doi:10.1029/2010WR009164.

[32] Bertin, S., & Friedrich, H. (2018). Effect of surface texture and structure on the development of stable fluvial armors. Geomorphology, 306, 64–79. doi:10.1016/j.geomorph.2018.01.013.

[33] Berni, C., Perret, E., & Camenen, B. (2018). Characteristic time of sediment transport decrease in static armour formation. Geomorphology, 317, 1–9. doi:10.1016/j.geomorph.2018.04.004.

[34] Ardiclioglu, M., Selenica, A., Ozdin, S., Kuriqi, A., & Genç, O. (2013, July). Investigation of average shear stress in natural stream. International Balkans Conference on Challenges of Civil Engineering (BCCCE), 19-21 May, 2011, Tirana, ALBANIA.

[35] Te Chow, V., (1964). Applied Hydrology, International. McGraw-Hill, New York, United States.